Superconducting spiral phase in the two-dimensional *t-J* model

Oleg P. Sushkov*
School of Physics, University of New South Wales, Sydney 2052, Australia

Valeri N. Kotov†
Institute of Theoretical Physics, University of Lausanne, CH-1015 Lausanne, Switzerland
(Received 28 October 2003; published 12 July 2004)

We analyze the $t-t'-t''-J$ model, relevant to the superconducting cuprates. By using chiral perturbation theory we have determined the ground state to be a spiral for small doping $\delta \ll 1$ near half filling. In this limit the solution does not contain any uncontrolled approximations. We evaluate the spin-wave Green's functions and address the issue of stability of the spiral state, leading to the phase diagram of the model. At $t'=t''=0$ the spiral state is unstable towards a local enhancement of the spiral pitch, and the nature of the true ground state remains unclear. However, for values of t' and t'' corresponding to real cuprates the (1,0) spiral state is stabilized by quantum fluctuations ("order from disorder" effect). We show that at $\delta \approx 0.119$ the spiral is commensurate with the lattice with a period of eight lattice spacings. It is also demonstrated that spin-wave mediated superconductivity develops in the spiral state and a lower limit for the superconducting gap is derived. Even though one cannot classify the gap symmetry according to the lattice representations $(s,p,d,\ldots)$ since the symmetry of the lattice is spontaneously broken by the spiral, the gap always has lines of nodes along the $(1,\pm 1)$ directions.

DOI: 10.1103/PhysRevB.70.024503 PACS number(s): 11.30.Er, 31.30.Jv, 31.30.Gs

I. INTRODUCTION

The *t-J* model has been suggested to describe the essential low-energy physics of the high-T_c cuprates.[1–3] Formation of spirals in the doped *t-J* model was proposed by Shraiman and Siggia.[4] They showed that the pitch of the spiral is proportional to the hole concentration δ, see also Ref. 5. The idea that the spiral state is the ground state of the doped Heisenberg antiferromagnet attracted the attention of theorists,[6–13] however, the question of stability of the state remained controversial. According to Refs. 6, 8, and 10 the spiral state is unstable toward a local enhancement of the spiral pitch. On the other hand the analysis of Ref. 9 indicated that the spiral state is stable. A semiclassical analysis of stability of the (1,0) spiral state was performed in Ref. 5. According to this analysis the state is marginal (zero stiffness), which effectively indicates that the state is unstable. A complete stability analysis of spiral states in the Hubbard model was performed in Ref. 11 also using the semiclassical approximation. According to their analysis in the leading in powers of doping approximation the (1,1) spiral is always unstable and the (1,0) spiral is always marginal in agreement with Ref. 5. Recently the interest in the spiral state was renewed because of the strong experimental indications that at small doping the cuprates behave as spin glasses or even exhibit some kind of magnetic ordering. A summary of the available experimental data on one of the superconducting cuprates, $La_{2-\delta}Sr_{\delta}CuO_4$, is given in Ref. 14. The data also show that magnetic ordering and superconductivity coexist. The spin glass behavior is consistent with the spiral scenario, since doping is not uniform the pitch of the spiral is varying from point to point and hence on large scales it leads to spin glass behavior.[15]

In the present work we analyze the stability of spiral states within the random-phase approximation (RPA). The approximation is parametrically justified for $\delta \ll 1$. In this part of the work on the technical side we follow the approach developed by Igarashi and Fulde.[9] However, contrary to them and in agreement with Refs. 6 and 8, we conclude that in the "pure" *t-J* model ($t'=t''=0$) the spiral state is unstable with respect to a local enhancement of the spiral pitch. We find that relatively small values of t' and t'' stabilize the spiral order, with a uniform hole distribution. Our results are then consistent with numerical (DMRG) results indicating that inhomogeneous (striped) phases disappear with the increase of further-neighbor hoppings.[16,17] In our approach the instability of the spiral is closely related to the fact that the hole dispersion is almost degenerate along the face of the magnetic Brillouin zone. As soon as the degeneracy is sufficiently lifted by t' and t'' the instability disappears, leading to a stable (1,0) spiral state. Within the semiclasical approximation the effective stiffness of this state is zero in agreement with Refs. 5 and 11. However, spin quantum fluctuations give rise to a nonzero positive stiffness and hence favor stability via an "order from disorder" mechanism. For parameter values corresponding to real cuprates, the pitch of the spiral is proportional to doping, and at $\delta \approx 0.119$ the spiral becomes commensurate with the lattice with period 8, in agreement with the experimental data of Tranquada *et al.*[18,19]

The possibility of *s* and *d* wave pairing between mobile holes due to a static distortion of the Neel background was pointed out in Ref. 20. Such a distortion leads to an infinite set of very shallow two-hole bound states.[21] In Ref. 22 it was shown, under the assumption that Neel order is preserved under doping, that in the *t-J* model there is spin-wave mediated superconducting pairing in all waves except the *s* wave. The pairing was found to be maximum in the *d* wave channel. A numerical calculation performed in Ref. 23 under the same assumption showed that the pairing was quite strong. However, the picture of pairing[22,23] was not consistent be-

cause the starting point of the analysis was the (unstable) Neel background. In the present paper, after proving the stability of the spiral state, we consider superconducting pairing on this state. Using an approach similar to that of Ref. 22 we find a superconducting pairing instability and show that the gap always has lines of nodes along $(1,\pm 1)$ directions. We estimate analytically the lower limit for the superconducting gap. One cannot classify the gap according to the lattice symmetry representations since the symmetry is spontaneously broken by the spiral.

In essence of the method we use is chiral perturbation theory which allows the treatment of strong interactions and is exact in the long wavelength limit.[24] The small parameter of the approach is doping near half filling, $\delta \ll 1$. We cannot determine reliably whether $\delta=0.15$, $\delta=0.1$, or $\delta=0.05$ is sufficiently small to justify our calculations, but we claim that at sufficiently small δ only the long-range dynamics is important and the approach is parametrically justified. The analysis of pairing within the chiral perturbation theory by construction complies with the Adler relation[25] and hence with the argument presented by Schrieffer[26] concerning pairing via exchange of Goldstone excitations.

The structure of the paper is as follows. In Sec. II we calculate the single hole dispersion and the quasiparticle residue for different values of t' and t''. To do so we use the self-consistent Born approximation. After that we perform the RPA analysis and demonstrate the instability of the Neel order, at arbitrary small hole concentrations, towards formation of spirals. In Sec. III we consider the hole dispersion in different spiral states and compare the total energies of the states. The RPA analysis of stability of the (1,0) spiral state is performed in Sec. IV, and in Sec. V we calculate the reduction of the spiral on-site magnetization due to doping. Section VI is devoted to the superconducting pairing in spiral states. We present our conclusions in Sec. VII.

II. SINGLE HOLE PROPERTIES AND RPA PROOF OF INSTABILITY OF THE NEEL ORDER UPON DOPING

The Hamiltonian of the $t-t'-t''-J$ model is

$$H = -t\sum_{\langle ij\rangle\sigma} c^{\dagger}_{i\sigma}c_{j\sigma} - t'\sum_{\langle ij_1\rangle\sigma} c^{\dagger}_{i\sigma}c_{j_1\sigma} - t''\sum_{\langle ij_2\rangle\sigma} c^{\dagger}_{i\sigma}c_{j_2\sigma} + J\sum_{\langle ij\rangle\sigma}\left(\mathbf{S}_i\mathbf{S}_j - \frac{1}{4}n_i n_j\right). \quad (1)$$

$c^{\dagger}_{i\sigma}$ is the creation operator of an electron with spin $\sigma(\sigma=\uparrow,\downarrow)$ at site i of the two-dimensional square lattice, $\langle ij\rangle$ represents nearest neighbor sites, $\langle ij_1\rangle$ next nearest neighbors (diagonal), and $\langle ij_2\rangle$ represents next nearest sites. The spin operator is $\mathbf{S}_i = 1/2\, c^{\dagger}_{i\alpha}\sigma_{\alpha\beta}c_{i\beta}$, and the number density operator is $n_i=\Sigma_\sigma\, c^{\dagger}_{i\sigma}c_{i\sigma}$. The size of the exchange measured in two magnon Raman scattering[27,28] is $J=125$ meV. Calculations of the hopping matrix elements have been performed by Andersen *et al.*[29] They consider a two-plane situation and the effective matrix elements are slightly different for symmetric and antisymmetric combinations of orbitals between planes. After averaging over these combinations we obtain: $t=386$ meV, $t'=-105$ meV, $t''=86$ meV. From now on we set $J=1$. In these units we have

$$t=3.1, \quad t'=-0.8, \quad t''=0.7. \quad (2)$$

An analysis of angle-resolved-photoemission spectra for the insulating copper oxide $Sr_2CuO_2Cl_2$ performed in Ref. 30 with the Hamiltonian (1) and (2) shows an excellent agreement with experiment for both the single-hole dispersion and for the photoemission intensity. This analysis is based on the self-consistent born approximation (SCBA).[31,32] The approximation works very well due to the absence of single loop corrections to the hole-spin-wave vertex.[33,34] In the present calculation of single-hole properties we follow the approach of Ref. 30 and use the SCBA.

It is well known that without doping (half filling) the Hamiltonian (1) is equivalent to the two-dimensional (2D) Heisenberg model which has antiferromagnetic (Neel) order. There are two sublattices: sublattice a with spin up and sublattice b with spin down. Hence a hole created in the system has a pseudospin index a or b. The bare hole operator d_i is defined so that $d^{\dagger}_i \propto c_{i\uparrow}$ on the a sublattice and $\propto c_{i\downarrow}$ on the b sublattice. In the momentum representation

$$d^{\dagger}_{\mathbf{k}a} = \sqrt{\frac{2}{N(1/2+m)}}\sum_{i\in\uparrow} c_{i\uparrow}e^{i\mathbf{k}\mathbf{r}_i},$$

$$d^{\dagger}_{\mathbf{k}b} = \sqrt{\frac{2}{N(1/2+m)}}\sum_{j\in\downarrow} c_{j\downarrow}e^{i\mathbf{k}\mathbf{r}_j}, \quad (3)$$

where N is the number of sites and $m=|\langle 0|S_{iz}|0\rangle| \approx 0.3$ is the average sublattice magnetization. The quasimomentum $\mathbf{k}$ is limited to be inside the magnetic Brillouin zone: $\gamma_{\mathbf{k}} = \frac{1}{2}(\cos k_x + \cos k_y) \geqslant 0$. The index a (b) can be considered as pseudospin. Rotational invariance is spontaneously broken, but nevertheless the pseudospin gives the correct value of the spin z projection, a corresponds to $S_z=-1/2$ and b corresponds to $S_z=+1/2$. The coefficients in Eq. (3) provide the correct normalization

$$\langle 0|d_{\mathbf{k}\downarrow}d^{\dagger}_{\mathbf{k}\downarrow}|0\rangle = \frac{2}{N(1/2+m)}\sum_{i\in\uparrow}\langle 0|c^{\dagger}_{i\uparrow}c_{i\uparrow}|0\rangle = \frac{1}{1/2+m}\langle 0|\frac{1}{2}+S_{iz}|0\rangle = 1. \quad (4)$$

For spin excitations the usual linear spin-wave theory is used (see, e.g., the review paper[35]). Spin-wave excitations are described by operators $\alpha^{\dagger}_{\mathbf{q}}$ and $\beta^{\dagger}_{\mathbf{q}}$ creating spin waves with $S_z=-1$ and $S_z=+1$, respectively. The momentum $\mathbf{q}$ is restricted inside the magnetic Brillouin zone. The operators are defined by the equations

$$\sqrt{\frac{2}{N}}\sum_{i\in\uparrow} S_i^+ e^{-i\mathbf{q}\mathbf{r_i}} \approx u_\mathbf{q}\alpha_\mathbf{q} + v_\mathbf{q}\beta_{-\mathbf{q}}^\dagger,$$

$$\sqrt{\frac{2}{N}}\sum_{j\in\downarrow} S_j^- e^{i\mathbf{q}\mathbf{r_j}} \approx v_\mathbf{q}\alpha_\mathbf{q}^\dagger + u_\mathbf{q}\beta_{-\mathbf{q}}. \quad (5)$$

The spin-wave dispersion and the parameters of the Bogoliubov transformation diagonalizing the spin-wave Hamiltonian are

$$\omega_\mathbf{q} = 2\sqrt{1-\gamma_\mathbf{q}^2},$$

$$u_\mathbf{q} = \sqrt{\frac{1}{\omega_\mathbf{q}} + \frac{1}{2}},$$

$$v_\mathbf{q} = -\,\mathrm{sgn}(\gamma_\mathbf{q})\sqrt{\frac{1}{\omega_\mathbf{q}} - \frac{1}{2}}. \quad (6)$$

Hopping to a nearest-neighbor site in the Hamiltonian (1) leads to an interaction of the hole with the spin-waves

$$H_{h,sw} = \sum_{\mathbf{k},\mathbf{q}} g_{\mathbf{k},\mathbf{q}}(d_{\mathbf{k}+\mathbf{q}a}^\dagger d_{\mathbf{k}b}\alpha_\mathbf{q} + d_{\mathbf{k}+\mathbf{q}b}^\dagger d_{\mathbf{k}a}\beta_\mathbf{q} + \mathrm{H.c.}), \quad (7)$$

with the vertex $g_{\mathbf{k},\mathbf{q}}$ given by Refs. 33 and 34

$$g_{\mathbf{k},\mathbf{q}} \equiv \langle 0|\alpha_\mathbf{q} d_{\mathbf{k}b}|H_t|d_{\mathbf{k}+\mathbf{q}a}^\dagger|0\rangle = 4t\sqrt{\frac{2}{N}}(\gamma_\mathbf{k}u_\mathbf{q} + \gamma_{\mathbf{k}+\mathbf{q}}v_\mathbf{q}). \quad (8)$$

The vertex $g_{\mathbf{k},\mathbf{q}}$ is independent of t', t'' because these parameters correspond to hopping inside one sublattice. In agreement with Adler relation[25] the vertex vanishes at $q\to 0$. We calculate the hole Green's function using the SCBA approximation.[31–34] This gives the quasiparticle dispersion $\epsilon_\mathbf{k}$ and the quasiparticle residue $Z_\mathbf{k}$. In the vicinity of the dispersion minima, $\mathbf{k}_0=(\pm\pi/2,\pm\pi/2)$, the quasiparticle residue is

$$Z_\mathbf{k} \approx Z \equiv Z_{\mathbf{k}_0}, \quad (9)$$

and the dispersion can be approximated as

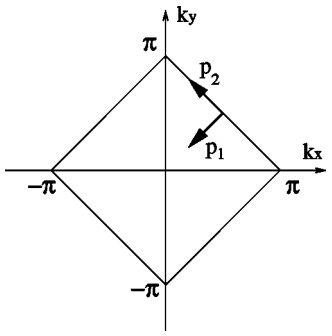

FIG. 1. Magnetic Brillouin zone.

$$\epsilon_\mathbf{k} \approx \mathrm{const} + \beta_1\gamma_\mathbf{k}^2 + \beta_2(\gamma_\mathbf{k}^-)^2 \approx \mathrm{const} + \beta_1\frac{p_1^2}{2} + \beta_2\frac{p_2^2}{2} \to \beta_1\frac{p_1^2}{2} + \beta_2\frac{p_2^2}{2}. \quad (10)$$

Here $\gamma_\mathbf{k}^- = \frac{1}{2}(\cos k_x - \cos k_y)$, $\mathbf{p}=\mathbf{k}-\mathbf{k}_0$, the component p_1 is orthogonal to the face of the Brillouin zone and the component p_2 is parallel to the face, see Fig. 1. The results of our calculations at $t=3.1$ and for the second neighbor hoppings within the intervals $-1<t'<0$ and $0<t''<1$ can be fitted as

$$t = 3.1,$$

$$\beta_1 = 1.96 + 1.15t' + 0.06t'^2 + 2.70t'' + 0.53t''^2 + 0.50t't'',$$

$$\beta_2 = 0.30 - 1.33t' - 0.19t'^2 + 2.80t'' + 1.06t''^2 - 0.14t't'',$$

$$Z = 0.29 + 0.055t' + 0.195t''. \quad (11)$$

These formulae agree with the results of Refs. 33 and 34 at $t'=t''=0$, as well as with Ref. 30 for t', t'' given by Eq. (2). The quasiparticle-spin-wave interaction differs from the bare interaction (7) only by the presence of the quasiparticle residues and reads

$$H_{qp,sw} = \sum_{\mathbf{k},\mathbf{q}} M_\mathbf{q}(h_{\mathbf{k}+\mathbf{q}a}^\dagger h_{\mathbf{k}b}\alpha_\mathbf{q} + h_{\mathbf{k}+\mathbf{q}b}^\dagger h_{\mathbf{k}a}\beta_\mathbf{q} + \mathrm{H.c.}), \quad (12)$$

where $h_{\mathbf{k}a}^\dagger$ and $h_{\mathbf{k}b}^\dagger$ are quasihole creation operators, and the vertex $M_\mathbf{q}$ has the form (we set $N=1$ for convenience)

$$M_\mathbf{q} = \sqrt{Z_\mathbf{k}Z_{\mathbf{k}+\mathbf{q}}}g_{\mathbf{k},\mathbf{q}} \approx -\,2^{7/4}Zt\frac{q_1}{\sqrt{q}}. \quad (13)$$

Here q_1 is the component of $\mathbf{q}$ orthogonal to the face of the Brillouin zone, and we assume that $\mathbf{k}\approx\mathbf{k}_0$ and $q\ll 1$.

It is convenient to introduce the fields $\pi_\mathbf{q}$ and $\lambda_\mathbf{q}$ instead of $\alpha_\mathbf{q}$ and $\beta_\mathbf{q}$

$$\pi_\mathbf{q} = \alpha_\mathbf{q} - \beta_{-\mathbf{q}}^\dagger,$$

$$\lambda_\mathbf{q} = \alpha_\mathbf{q} + \beta_{-\mathbf{q}}^\dagger. \quad (14)$$

The Green's functions of these fields are defined as

$$D_{\pi n}(\omega,\mathbf{q}) = -\,i\int_{-\infty}^{+\infty} dt e^{i\omega t}\langle T[\pi_\mathbf{q}(t)\pi_\mathbf{q}^\dagger(0)]\rangle,$$

$$D_{\lambda n}(\omega,\mathbf{q}) = -\,i\int_{-\infty}^{+\infty} dt e^{i\omega t}\langle T[\lambda_\mathbf{q}(t)\lambda_\mathbf{q}^\dagger(0)]\rangle. \quad (15)$$

In the absence of interactions they are

$$D_{\pi n}^{(0)}(\omega,\mathbf{q}) = D_{\lambda n}^{(0)}(\omega,\mathbf{q}) = \frac{2\omega_\mathbf{q}}{\omega^2 - \omega_\mathbf{q}^2 + i0}. \quad (16)$$

The index n in Eqs. (15) and (16) labels them as normal Green's functions. According to Eq. (12) the field $\pi_\mathbf{q}$ interacts with the quasiholes:

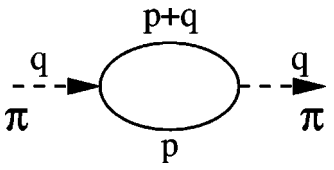

FIG. 2. $\pi_{\mathbf{q}}$-spin-wave polarization operator.

$$H_{qp,\pi} = \sum_{\mathbf{k},\mathbf{q}} M_{\mathbf{q}}(h^{\dagger}_{\mathbf{k}+\mathbf{q}a} h_{\mathbf{k}b} \pi_{\mathbf{q}} + \text{H.c.}), \tag{17}$$

while the field $\lambda_{\mathbf{q}}$ remains idle with respect to this interaction. The interaction (17) generates a loop correction to the spin-wave Green's function shown in Fig. 2. The holes are fermions and occupy four half pockets or two full pockets as shown in Fig. 3. At a given momentum there are two states with different pseudospin, so the Fermi energy ϵ_F and the total Fermi motion energy E_F (per lattice site) read

$$\epsilon_F = \frac{\pi}{2}\sqrt{\beta_1\beta_2}\delta,$$

$$E_F = \frac{\pi}{4}\sqrt{\beta_1\beta_2}\delta^2, \tag{18}$$

where $\delta \ll 1$ is the hole concentration. The calculation of the polarization operator Fig. 2 is straightforward and gives

$$P(\omega = i\xi, \mathbf{q}) = \sum_{pockets} M^2_{\mathbf{q}} \sum_{\mathbf{p}} \frac{2(\epsilon_{\mathbf{p}} - \epsilon_{\mathbf{p}+\mathbf{q}}) n_{\mathbf{p}}(1 - n_{\mathbf{p}+\mathbf{q}})}{\xi^2 + (\epsilon_{\mathbf{p}+\mathbf{q}} - \epsilon_{\mathbf{p}})^2}$$
$$= -\frac{2^{5/2} Z^2 t^2}{\pi\sqrt{\beta_1\beta_2}} \frac{1}{q} \sum_{pockets} q_1^2 F(\xi, \mathbf{q}),$$

$$F(\xi, \mathbf{q}) = \frac{1}{t^2}[t^2 - 2Re\sqrt{(t^2/2 + i\xi)^2 - 2\epsilon_F t^2}], \quad F(0,0) = 1. \tag{19}$$

Here $t^2 = \beta_1 q_1^2 + \beta_2 q_2^2$ and $n_{\mathbf{p}}$ is the Fermi distribution function. Re stays for real part. Summation over two full pockets shown on the right side of Fig. 3 has to be performed. Note

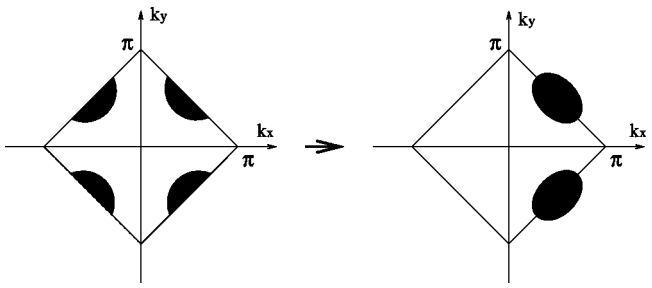

FIG. 3. Hole pockets and Fermi surface for the Neel state and for the spiral state with $\mathbf{Q} \propto (1,0)$.

that what is q_1 for one pocket is q_2 for the other, and vice versa. At $\omega = 0$ and $q \ll p_F \sim \sqrt{\delta}$ the polarization operator (19) is particularly simple:

$$P(0, \mathbf{q}) = -\frac{2^{5/2} Z^2 t^2}{\pi\sqrt{\beta_1\beta_2}} q. \tag{20}$$

The polarization operator is always proportional to q, as a direct consequence of Goldstone's theorem. A crucial point is that the polarization operator (20) is independent of δ. Taking into account the one-loop diagram (Fig. 2) the π-magnon Green's function (15) becomes

$$D_{\pi n}(\omega, \mathbf{q}) = \frac{2\omega_{\mathbf{q}}}{\omega^2 - \omega^2_{\mathbf{q}} - 2\omega_{\mathbf{q}} P(\omega, \mathbf{q}) + i0}. \tag{21}$$

The stability of the system requires that all poles of the Green's function (21) are at positive ω^2. Using Eqs. (20) and (11) one can see that this criterion is violated for $q \ll p_F \sim \sqrt{\delta}$ at arbitrary small doping, because (cf. with Refs. 11 and 36)

$$\omega^2_{\mathbf{q}} + 2\omega_{\mathbf{q}} P(\omega = 0, \mathbf{q}) = 2q^2\left(1 - \frac{8Z^2 t^2}{\pi\sqrt{\beta_1\beta_2}}\right) < 0. \tag{22}$$

This result signals an instability towards formation of spirals.

In the presented RPA proof of the Neel state instability we have used the following approximations: (1) The single hole properties (dispersion and quasiparticle residue) have been calculated without account of other holes. (2) The incoherent part of the hole Green's function has been neglected. (3) Interactions between quasiholes have been neglected. These approximations are *parametrically* justified at sufficiently small δ since Eq. (20) is independent of δ. We observe that doping influences the behavior of the system only at momenta $q \sim \sqrt{\delta} \ll 1$. At the same time all integrals in the SCBA are convergent at large momenta, $q \sim 1$. Consequently doping gives a negligible correction ($\propto \delta$) to the dispersion. The same is true for the incoherent part of the hole Green's function and for the hole-hole interaction. The leading correction from these effects is $\propto \delta \ln \delta$, see Ref. 37, and hence it is also negligible for sufficiently small δ.

III. SPIRAL STATES, HOLE DISPERSION, AND TOTAL ENERGY

In a spiral state there are still two sublattices, sublattice a and sublattice b, but the spin at every site j of each sublattice is rotated by an angle θ_j:

$$|\psi_j\rangle = e^{i\theta_j \mathbf{n}\cdot\sigma/2}|\uparrow\rangle \quad \text{if } j \in a \text{ sublattice},$$

$$|\psi_j\rangle = e^{i\theta_j \mathbf{n}\cdot\sigma/2}|\downarrow\rangle \quad \text{if } j \in b \text{ sublattice},$$

$$\theta_j = \mathbf{Q}\cdot\mathbf{r}_j. \tag{23}$$

Here $\mathbf{Q} \ll 1$ is the vector of the spiral, σ is the vector of Pauli matrices, and $\mathbf{n}$ is an axis of rotation. The direction of $\mathbf{n}$ can be arbitrary in the plane orthogonal to the spin $|\uparrow\rangle$ in Eq. (23), $\mathbf{n} = (n_1, n_2, 0) = (\cos\alpha, \sin\alpha, 0)$. To first order in Q the small rotation (23) does not influence the spin-wave disper-

sion and the hole-spin-wave interaction considered in the preceding section. The only effect which appears at first order in Q is the possibility for a hole to hop between nearest-neighbor sites of the lattice. Using Eqs. (1) and (23) one can easily find the Hamiltonian describing this hopping:

$$H_Q = -t \sum_{\xi, i\in a} \sin\left(\frac{\mathbf{Q}\cdot\xi}{2}\right)[ie^{-i\alpha} d^\dagger_{i+\xi,b} d_{ia} - ie^{i\alpha} d^\dagger_{ia} d_{i+\xi,b}]. \tag{24}$$

Here ξ is a lattice vector directed from a given site $i\in a$ to the nearest neighbor $i+\xi\in b$. One can rewrite Eq. (24) in momentum representation using the quasihole operators $h_{\mathbf{k}}$:

$$H_Q = -t\sum_{\mathbf{k}} (Q_x \sin k_x + Q_y \sin k_y)(e^{-i\alpha} d^\dagger_{\mathbf{k}b} d_{\mathbf{k}a} + e^{i\alpha} d^\dagger_{\mathbf{k}a} d_{\mathbf{k}b})$$
$$\to -Z_{\mathbf{k}} t \sum_{\mathbf{k}} (Q_x \sin k_x + Q_y \sin k_y)(e^{-i\alpha} h^\dagger_{\mathbf{k}b} h_{\mathbf{k}a} + e^{i\alpha} h^\dagger_{\mathbf{k}a} h_{\mathbf{k}b}). \tag{25}$$

The quasiparticle residue $Z_{\mathbf{k}}$ is exactly the same as the one found in the preceding section by the SCBA. Indeed, the effects considered in the present section are relevant to the long-range dynamics, so the corresponding momenta are very small, $Q\propto\delta\ll 1$. On the other hand all the integrals in the SCBA are convergent at large momenta and therefore not sensitive to the long-range dynamics. The axes x and y coincide with the crystal axes. Note that the axes 1 and 2 used to define the phase α are not related to the crystal axes. The Hamiltonian (25) mixes the states $h^\dagger_{\mathbf{k}a}$ and $h^\dagger_{\mathbf{k}b}$. Therefore the effective Hamiltonian matrix for a given $\mathbf{k}$ takes the form

$$H_{eff} = \begin{pmatrix} \epsilon_{\mathbf{k}} & -Z_{\mathbf{k}} t e^{-i\alpha}[Q_x \sin k_x + Q_y \sin k_y] \\ -Z_{\mathbf{k}} t e^{i\alpha}[Q_x \sin k_x + Q_y \sin k_y] & \epsilon_{\mathbf{k}} \end{pmatrix}, \tag{26}$$

where $\epsilon_{\mathbf{k}}$ is found in the preceding section. In the vicinity of the points $\mathbf{k}_0=(\pm\pi/2, \pm\pi/2)$ one can use Eqs. (9) and (10) and hence H_{eff} takes the following form:

$$H_{eff} = \begin{pmatrix} \epsilon_{\mathbf{k}} & \sqrt{2} Z t e^{-i\alpha} Q_1 \\ \sqrt{2} Z t e^{i\alpha} Q_1 & \epsilon_{\mathbf{k}} \end{pmatrix}, \tag{27}$$

where Q_1 is the component of $\mathbf{Q}$ orthogonal to the corresponding face of the magnetic Brillouin zone. We denote by $\psi^\dagger_{\mathbf{k}}$ and $\varphi^\dagger_{\mathbf{k}}$ the creation operators that diagonalize this Hamiltonian

$$\psi^\dagger_{\mathbf{k}} = \frac{1}{\sqrt{2}}(h^\dagger_{\mathbf{k}a} - e^{-i\mu} h^\dagger_{\mathbf{k}b}),$$

$$\varphi^\dagger_{\mathbf{k}} = \frac{1}{\sqrt{2}}(h^\dagger_{\mathbf{k}a} + e^{-i\mu} h^\dagger_{\mathbf{k}b}), \tag{28}$$

where $e^{i\mu}=(Q_1/|Q|)e^{i\alpha}$. The corresponding dispersions are

$$\epsilon_{\mathbf{k}-} = \epsilon_{\mathbf{k}} - \sqrt{2} Z t |Q_1|,$$

$$\epsilon_{\mathbf{k}+} = \epsilon_{\mathbf{k}} + \sqrt{2} Z t |Q_1|. \tag{29}$$

We will see that $|Q_1|$ is always large enough, so only the states corresponding to the $\epsilon_{\mathbf{k}-}$ branch (ψ band) are filled by holes. According to Eq. (29) the total kinetic-energy gain due to the spiral is $\Delta E_{kin} = -\sqrt{2} Z t |Q_1| \delta$ per lattice site. On the other hand the spiral increases the magnetic energy. The variation of the magnetic energy per lattice site is $\Delta E_{magn} = \frac{1}{2}\rho_s Q^2$, where $\rho_s = Z_\rho/4 \approx 0.18$ sis the spin stiffness, and $Z_\rho \approx 0.72$ is the renormalization factor due to higher $1/S$-corrections.[38] Finally, the Fermi motion of holes $E_F \propto \delta^2$, also contribute to the total energy. Altogether the total energy of the spiral state (per site) with respect to the undoped antiferromagnet is

$$E = \tfrac{1}{2}\rho_s Q^2 - \sqrt{2} Z t |Q_1| \delta + E_F. \tag{30}$$

There are two possibilities to minimize the total energy: for a spiral directed along a diagonal of the lattice $\mathbf{Q}\propto(1,1)$, and for a spiral directed along a crystal axis of the lattice $\mathbf{Q}\propto(1,0)$. For the diagonal spiral the effective Fermi surface consists of two half pockets or one whole pocket, see Fig. 4. The hole states do not have a pseudospin index and hence the Fermi energy ϵ_F and the total Fermi motion energy E_F (per site) in this case $[\mathbf{Q}\propto(1,1)]$ read:

$$\epsilon_F = 2\pi\sqrt{\beta_1\beta_2}\,\delta,$$

$$E_F = \pi\sqrt{\beta_1\beta_2}\,\delta^2. \tag{31}$$

For the spiral along a crystal axis the effective Fermi surface consists of four half pockets or two whole pockets, similarly

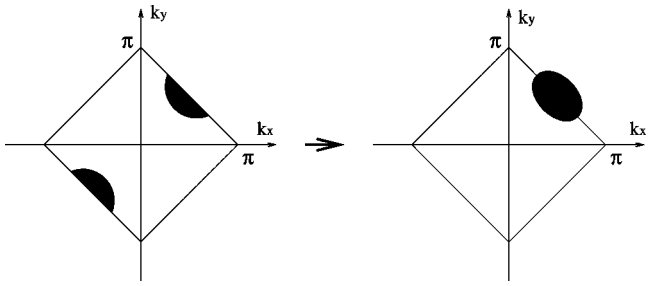

FIG. 4. Hole pockets and Fermi surface for the spiral state with $\mathbf{Q}\propto(1,1)$.

to the Neel case, see Fig. 3. However, the hole states in a spiral do not carry a pseudospin index and hence the Fermi energy and the total Fermi motion energy E_F in this case $[\mathbf{Q} \propto (1,0)]$ are

$$\epsilon_F = \pi\sqrt{\beta_1\beta_2}\delta,$$

$$E_F = \frac{\pi}{2}\sqrt{\beta_1\beta_2}\delta^2. \quad (32)$$

Using Eqs. (30)–(32) we find the following expressions for the energy of the spiral state relative to the energy of the undoped antiferromagnet:

$$\mathbf{Q} \propto (1,1): E_{(1,1)} = \tfrac{1}{2}\rho_s Q^2 - \sqrt{2}ZtQ\delta + \pi\sqrt{\beta_1\beta_2}\delta^2,$$

$$\mathbf{Q} \propto (1,0): E_{(1,0)} = \frac{1}{2}\rho_s Q^2 - ZtQ\delta + \frac{\pi}{2}\sqrt{\beta_1\beta_2}\delta^2. \quad (33)$$

Minimizing E with respect to Q one finds

$$\mathbf{Q} \propto (1,1): \quad Q = \frac{\sqrt{2}Zt}{\rho_s}\delta, \quad E_{(1,1)} = \left\{-\frac{Z^2t^2}{\rho_s} + \pi\sqrt{\beta_1\beta_2}\right\}\delta^2,$$

$$\mathbf{Q} \propto (1,0): \quad Q = \frac{Zt}{\rho_s}\delta, \quad E_{(1,0)} = \left\{-\frac{Z^2t^2}{2\rho_s} + \frac{\pi}{2}\sqrt{\beta_1\beta_2}\right\}\delta^2. \quad (34)$$

Equations (33) and (34) agree with Ref. 9, see also Ref. 39. We see that $E_{(1,1)}=2E_{(1,0)}$, so if these energies are positive then the state (1,0) has lower energy than the (1,1) state. It should be noted that the energy $E_{(1,0)}$ is always lower than the energy of the doped Neel state (i.e., the difference between $E_{(1,0)}$ and Eq. (18) is always negative). When $E_{(1,1)}$ is negative then this state has lower energy. However, in this case the corresponding compressibility $(\partial^2 E_{(1,1)}/\partial\delta^2)$ is also negative which implies an instability towards a state with an inhomogeneous charge distribution. Consequently the (1,1) spiral state is always unstable in agreement with the conclusions of Refs. 6, 8, and 11. On the other hand the compressibility of the (1,0) state is always positive (in agreement with Ref. 11). Using the results of our SCBA calculations, summarized in Eq. (11), as well as Eq. (34), one can easily find the region where the state (1,0) is realized. Our results are summarized in Fig. 5. The energy $E_{(1,0)}$ vanishes along the solid line, and the spiral state is unstable in the right bottom corner of the phase diagram. To complete the analysis of stability of the (1,0) spiral state we must calculate the spin-wave polarization operator ("transverse stiffness"). We leave this analysis to the following section.

For values of t, t', and t'' from Ref. 29, Eq. (2), the (1,0) spiral is stable. At this point $Z=0.38$, Eq. (11), and hence according to Eq. (34) the magnitude of the spiral vector is

$$Q = 6.58\delta \quad \text{at} \quad t = 3.1, \quad t' = -0.8, \quad t'' = 0.7. \quad (35)$$

The spiral is commensurate with the lattice if $Qn=\pi$, where n is an integer number. The corresponding hole concentration $\delta_n = \pi/(6.58n)$. This results in an effective antiferromagnetic structure with period Δr. The period is $\Delta r = n$ for odd values of n, and $\Delta r = 2n$ for even values of n. In Table I we present the values of δ_n and the corresponding periods of the commensurate antiferromagnetic structure for several values of n.

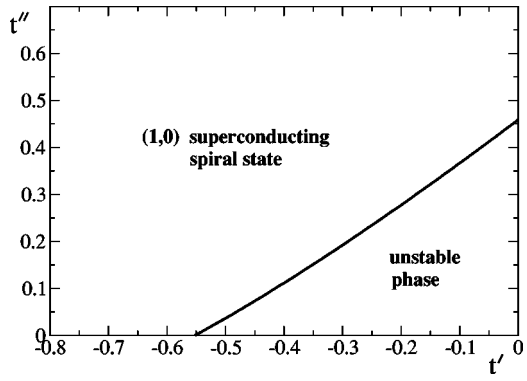

FIG. 5. Phase diagram of the t-t'-t''-J model at t=3.1 and small doping, $\delta \ll 1$. The bottom right corner corresponds to the pure t-J model, $t'=t''=0$. The top left corner corresponds to parameters from Ref. 29, Eq. (2). The region of stability of the superconducting (1,0) spiral phase is shown.

Notice that for $\delta_n=0.119$ the period is 8, in agreement with experimental data.[18] The spin structure at this doping value is shown in Fig. 6. In Sec. VII we discuss further the possible connections of our results to the physics of the superconducting cuprates.

IV. SPIN-WAVE GREEN'S FUNCTION IN THE SPIRAL STATE AND RPA STABILITY ANALYSIS OF THE STATE

The stability analysis of the (1,0) spiral state requires a calculation of the spin-wave Green's functions (15), similar to the calculation performed in Sec. II for the Neel state. The spin wave $\lambda_{\mathbf{q}}$, Eq. (14), remains unchanged since it does not interact with the holes. The interaction of the spin wave $\pi_{\mathbf{q}}$ with the holes is given by Eq. (17), but one has to take into account the fact that the correct quasiparticle states are represented by the operators $\psi_{\mathbf{k}}$ and $\varphi_{\mathbf{k}}$ instead of $h_{\mathbf{k}a}$ and $h_{\mathbf{k}b}$, Eq. (28). The diagrams shown in Fig. 7 contribute to the π-spin-wave polarization operators. The diagrams in Figs. 7(A) and 7(B) contribute to the normal polarization operator. The filled state is always $\psi_{\mathbf{k}}$, however, the excited state in the loop can be either $\psi_{\mathbf{k}+\mathbf{q}}$ or $\varphi_{\mathbf{k}+\mathbf{q}}$, see Eq. (28), providing the difference between the diagrams in Figs. 7(A) and 7(B). Since pseudospin is not conserved there is also an anomalous polarization operator. The contributions to the anomalous operator are given by the diagrams in Figs. 7(C) and 7(D). The

TABLE I. Values of the hole concentration δ_n at which a commensurate antiferromagnetic structure with period Δr is established.

n	3	4	5	6
δ_n	0.159	0.119	0.095	0.079
Δr	3	8	5	12

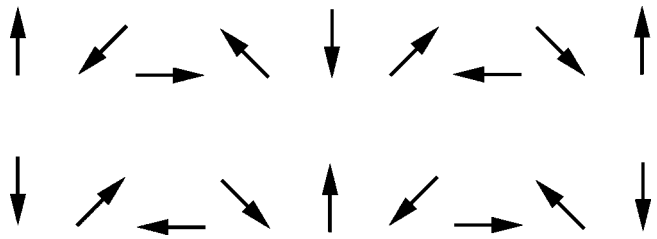

FIG. 6. (1,0) Spiral state for $\delta=0.119$, corresponding to $Q=\pi/4$.

anomalous polarization operator gives rise to the anomalous π-spin-wave Green's function defined as

$$D_{\pi a}(\omega,\mathbf{q}) = -i\int_{-\infty}^{+\infty} dt e^{i\omega t}\langle T[\pi^{\dagger}_{-\mathbf{q}}(t)\pi^{\dagger}_{\mathbf{q}}(0)]\rangle. \tag{36}$$

A straightforward calculation of the polarization operators P_A and P_C, taking into account transitions within the same subband, gives (we set $\omega=i\xi$ from now on)

$$\begin{aligned} P_A(i\xi,\mathbf{q}) &= -e^{2i\mu}P_C(i\xi,\mathbf{q}) \\ &= \sum_{pockets}\frac{M_{\mathbf{q}}^2}{4}\sum_{\mathbf{p}}\frac{2(\epsilon_{\mathbf{p}}-\epsilon_{\mathbf{p}+\mathbf{q}})n_{\mathbf{p}}(1-n_{\mathbf{p}+\mathbf{q}})}{\xi^2+(\epsilon_{\mathbf{p}+\mathbf{q}}-\epsilon_{\mathbf{p}})^2} \\ &= -\frac{\sqrt{2}Z^2t^2}{\pi\sqrt{\beta_1\beta_2}}\frac{1}{q}\sum_{pockets} q_1^2 F(\xi,\mathbf{q}). \end{aligned} \tag{37}$$

The function $F(\xi,\mathbf{q})$ is defined in Eq. (19). Equation (37) differs from Eq. (19) by the coefficient 1/4 only. The summation has to be performed over two full pockets of the (1,0) spiral state, Fig. 3. We remind the reader that q_1 is the component orthogonal to the face of the Brillouin zone. Next we evaluate the polarization operators P_B and P_D describing transitions between subbands

$$P_B(i\xi,\mathbf{q}) = e^{2i\mu}P_D(i\xi,\mathbf{q}) = \sum_{pockets}\frac{M_{\mathbf{q}}^2}{4}\sum_{\mathbf{p}}\frac{2(\epsilon_{\mathbf{p}}-\epsilon_{\mathbf{p}+\mathbf{q}}-\Delta)n_{\mathbf{p}}}{\xi^2+(\epsilon_{\mathbf{p}+\mathbf{q}}-\epsilon_{\mathbf{p}}+\Delta)^2}$$

$$= -\frac{\sqrt{2}Z^2t^2}{\pi\sqrt{\beta_1\beta_2}}\frac{1}{q}\sum_{pockets} q_1^2\Phi(\xi,\mathbf{q}),$$

$$\Phi(\xi,\mathbf{q}) = \frac{1}{t^2}[t^2+2\Delta-2\,\mathrm{Re}\sqrt{(t^2/2+\Delta+i\xi)^2-2\epsilon_F t^2}],$$

$$\Phi(0,0) = \frac{2\epsilon_F}{\Delta}, \tag{38}$$

where $\Delta=2\sqrt{2}Zt|Q_1|$ is the splitting between the subbands, see Eq. (29). Taking into account Eq. (34) for the (1,0) state we obtain

$$\Delta = \frac{2Z^2t^2}{\rho_s}\delta \approx 15\delta. \tag{39}$$

According to Fig. 7 and Eqs. (37) and (38) the normal and the anomalous polarization operators are

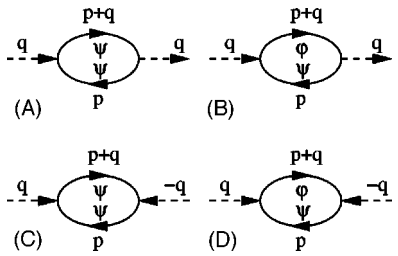

FIG. 7. Contributions to π-spin-wave polarization operators. (A) and (C) describe transitions within the ψ band, and (B) and (D) describe transitions between the ψ and φ bands.

$$\begin{aligned} P_n(i\xi,\mathbf{q}) &= P_A(i\xi,\mathbf{q}) + P_B(i\xi,\mathbf{q}) \\ &= -\frac{\sqrt{2}Z^2t^2}{\pi\sqrt{\beta_1\beta_2}}\frac{1}{q}\sum_{pockets} q_1^2[F(\xi,\mathbf{q})+\Phi(\xi,\mathbf{q})], \end{aligned}$$

$$\begin{aligned} P_a(i\xi,\mathbf{q}) &= P_C(i\xi,\mathbf{q}) + P_D(i\xi,\mathbf{q}) \\ &= -\frac{\sqrt{2}Z^2t^2}{\pi\sqrt{\beta_1\beta_2}}\frac{e^{-2i\mu}}{q}\sum_{pockets} q_1^2[-F(\xi,\mathbf{q})+\Phi(\xi,\mathbf{q})]. \end{aligned} \tag{40}$$

The corresponding Dyson's equations for the Green's functions read

$$\begin{aligned} D_{\pi n}(q) &= D^{(0)}_{\pi n}(q) + D^{(0)}_{\pi n}(q)P_n(q)D_{\pi n}(q) \\ &\quad + D^{(0)}_{\pi n}(q)P_a(q)D_{\pi a}(q), \end{aligned}$$

$$D_{\pi a}(q) = D^{(0)}_{\pi n}(-q)P_n(-q)D_{\pi a}(q) + D^{(0)}_{\pi n}(-q)P^{*}_a(q)D_{\pi n}(q), \tag{41}$$

with $D^{(0)}_{\pi n}$ given by Eq. (16). By solving these equations we obtain the normal and the anomalous Green's functions of the π field

$$D_{\pi n}(\omega=i\xi,\mathbf{q}) = \frac{-2\omega_{\mathbf{q}}[\xi^2+\omega_{\mathbf{q}}^2+2\omega_{\mathbf{q}}P_n(i\xi,\mathbf{q})]}{[\xi^2+\omega_{\mathbf{q}}^2+2\omega_{\mathbf{q}}P_n(i\xi,\mathbf{q})]^2-4\omega_{\mathbf{q}}^2|P_a(i\xi,\mathbf{q})|^2},$$

$$D_{\pi a}(\omega=i\xi,\mathbf{q}) = \frac{2\omega_{\mathbf{q}}P^{*}_a(i\xi,\mathbf{q})}{[\xi^2+\omega_{\mathbf{q}}^2+2\omega_{\mathbf{q}}P_n(i\xi,\mathbf{q})]^2-4\omega_{\mathbf{q}}^2|P_a(i\xi,\mathbf{q})|^2}. \tag{42}$$

As already discussed in Sec. II, a necessary condition for the stability of the system is the absence of poles in the Green's functions at negative ω^2 (positive ξ^2). The most dangerous is the regime of very low frequencies and momenta ($\omega\ll\epsilon_F$, $q\ll p_F\sim\sqrt{\delta}$). Therefore the criterion of stability is

$$[\omega_{\mathbf{q}}^2+2\omega_{\mathbf{q}}P_n(0,\mathbf{q})]^2 > 4\omega_{\mathbf{q}}^2|P_a(0,\mathbf{q})|^2. \tag{43}$$

Using Eq. (40) the stability criterion can be rewritten as

$$1 > \frac{2Z^2t^2}{\pi\sqrt{\beta_1\beta_2}}\left|1+\frac{\pi\sqrt{\beta_1\beta_2}\rho_s}{Z^2t^2}\right| + \frac{2Z^2t^2}{\pi\sqrt{\beta_1\beta_2}}\left|1-\frac{\pi\sqrt{\beta_1\beta_2}\rho_s}{Z^2t^2}\right|. \tag{44}$$

According to Eq. (34) the expression $1-\pi\sqrt{\beta_1\beta_2}\rho_s/Z^2t^2$ is negative in the $(1,0)$ phase since $E_{(1,0)}$ is positive. Therefore the criterion (44) reads

$$1-4\rho_s = 0.28 > 0, \tag{45}$$

meaning that the spiral phase is always stable. It is important to note that the phase is stable only due to spin-quantum fluctuations, and the stability is an order from disorder effect. Without account of the fluctuations (semiclassical approximation), $\rho_s = 1/4$, and hence the effective transverse stiffness vanishes, $1-4\rho_s = 0$. In this case the system becomes marginal, or in essence unstable, as pointed out in Refs. 5 and 11. Thus the spin quantum fluctuations make the (1,0) spiral phase stable. We stress that the spin quantum fluctuation effects in an undoped antiferromagnet are known quite accurately from numerous approaches (spin wave, series expansions, Monte Carlo, etc.). Within the chiral perturbation theory, used in the present work, one can express the leading terms in the hole density via the parameters of the undoped system. In this sense we perform an "exact" account of the quantum fluctuations. However, we do not calculate terms subleading in the hole density because such a calculation cannot be performed without uncontrolled mean-field approximations. It is possible that at sufficiently large doping the spiral phase becomes unstable due to such subleading terms. One possible type of instability is towards formation of a noncoplanar state, as suggested in Ref. 11. We cannot determine the exact value of doping δ which is small enough to justify our calculations, but we claim that at sufficiently small δ our approach is parametrically justified, and consequently Fig. 5 represents the phase diagram of the t-t'-t''-J model. We emphasize that in this regime the (1,0) spiral phase is stable for values of parameters corresponding to real cuprates.

V. ON-SITE MAGNETIZATION IN THE SPIRAL STATE

In the undoped t-J model the spins order in a staggered collinear pattern and the value of the staggered magnetization is

$$M = |\langle S^z\rangle| \approx 0.303. \tag{46}$$

In a spiral state the on-site magnetization follows a spiral pattern and besides that the value of the magnetization is reduced compared to Eq. (46). We calculate now the reduction of the magnetization. Using the spin-wave operators (5) and neglecting corrections proportional to $Q^2 \propto \delta^2$ one can rewrite the on-site magnetization in the following form:

$$\begin{aligned} M = \frac{1}{2}\langle S_a^z - S_b^z\rangle &= 0.303 - 2\sum_{\mathbf{q}}\frac{1}{\omega_{\mathbf{q}}}\langle[\alpha_{\mathbf{q}}^\dagger\alpha_{\mathbf{q}} + \beta_{\mathbf{q}}^\dagger\beta_{\mathbf{q}} - \gamma_{\mathbf{q}}(\alpha_{\mathbf{q}}\beta_{-\mathbf{q}} \\ &+ \alpha_{\mathbf{q}}^\dagger\beta_{-\mathbf{q}}^\dagger)]\rangle = 1 - 2\sum_{\mathbf{q}}\frac{1}{\omega_{\mathbf{q}}}\langle[\alpha_{\mathbf{q}}^\dagger\alpha_{\mathbf{q}} + \beta_{-\mathbf{q}}\beta_{-\mathbf{q}}^\dagger - \gamma_{\mathbf{q}}(\alpha_{\mathbf{q}}\beta_{-\mathbf{q}} \\ &+ \alpha_{\mathbf{q}}^\dagger\beta_{-\mathbf{q}}^\dagger)]\rangle. \end{aligned} \tag{47}$$

For small doping the deviation of M from the value (46) is due to quantum fluctuations at small momenta, $q \ll 1$. Hence one can replace $\gamma_{\mathbf{q}} \to 1$ and rewrite Eq. (47) in terms of π-field averages and then the normal Green's function Eqs. (14) and (15):

$$M \to 1 - 2\sum_{\mathbf{q}}\frac{1}{\omega_{\mathbf{q}}}\langle\pi_{\mathbf{q}}^\dagger\pi_{\mathbf{q}}\rangle = 1 - 2i\sum_{\mathbf{q}}\frac{1}{\omega_{\mathbf{q}}}D_{\pi n}(t=-0,\mathbf{q}). \tag{48}$$

Finally, using the explicit expression (42) for the Green's function we find the reduction of the on-site magnetization in a spiral:

$$M = 0.303 + \Delta M,$$

$$\Delta M = -4\sum_{\mathbf{q}}\int\frac{d\xi}{2\pi}\left\{\frac{\xi^2+\omega_{\mathbf{q}}^2+2\omega_{\mathbf{q}}P_n(i\xi,\mathbf{q})}{[\xi^2+\omega_{\mathbf{q}}^2+2\omega_{\mathbf{q}}P_n(i\xi,\mathbf{q})]^2-4\omega_{\mathbf{q}}^2|P_a(i\xi,\mathbf{q})|^2} - \frac{1}{\xi^2+\omega_{\mathbf{q}}^2}\right\}. \tag{49}$$

A straightforward numerical integration of this equation with parameters corresponding to Eq. (2) gives the on-site magnetization plotted in Fig. 8.

For hole concentration $\delta = 0.12$, corresponding to a commensurate spiral (Fig. 6), the value of the magnetization is $M \approx 0.06$. It is quite close to the reported experimental values in $La_{1.88}Sr_{0.12}CuO_4$ (Ref. 40) as well as $La_{1.48}Nd_{0.4}Sr_{0.12}CuO_4$ (Ref. 19). The overall decrease of M as a function of doping is also consistent with experiment.[41] We observe that the spiral state disappears at $\delta_c \approx 0.16$, beyond which point ($\delta > \delta_c$) spin rotational invariance is restored. The existence of a magnetic quantum critical point inside the superconducting region is an issue of considerable current interest[42] (the spiral states support superconductivity as discussed in Sec. VI). It has also been suggested that the phase emerging upon destruction of noncollinear magnetic order could be of RVB type and exhibit electron fractionalization,[42,43] although in the present work we can not address the structure of the magnetically disordered region $\delta > \delta_c$.

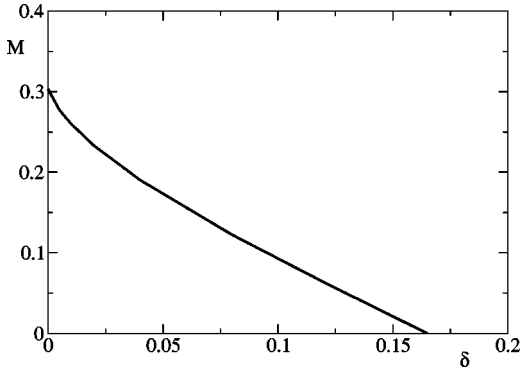

FIG. 8. On-site magnetization in the (1,0) spiral vs doping for $t=3.1$, $t'=-0.8$, and $t''=0.7$.

Using the expression for the polarization operator (40) one can show that ΔM can be expanded in powers of δ in the following way:

$$\Delta M = -a\delta \ln(1/\delta) + b\delta + c\delta^2 + \cdots . \tag{50}$$

This equation shows that the expansion is nonanalytic in δ. We have calculated the coefficients a and b (as well as c) numerically for several values of t' and t'', and tabulated them in Table II.

Only the logarithmic term in the expansion (50) is parametrically justified within the chiral perturbation theory which we use in the present work. This is due to the fact that the integral in Eq. (49) behaves as $\delta \int dq/q$ and consequently the "b" term in Eq. (50) is related to the upper limit of the integration, i.e., to the short-distance dynamics ($q \sim \pi$). Equation (49) overestimates the contribution of large momenta because it does not take into account the reduction of the quasiparticle residue away from $\mathbf{k}_0=(\pm\pi/2, \pm\pi/2)$. On the other hand it underestimates this contribution since it does not take into account the incoherent part of the hole Green's function. To estimate the uncertainty related to the short-distance dynamics we have calculated the reduction of the nearest-neighbor sites spin-spin correlator $\langle \mathbf{S}_i \cdot \mathbf{S}_j \rangle$ in the same way, i.e., assuming no variation of the quasiparticle residue and without the incoherent contribution. The result of this calculation agrees within 30% with the available numerical data.[44] This indicates that the values of the coefficient b in Table II are somewhat reliable. We stress once again that the leading "a" term in Eq. (50) is due to the long-distance dynamics only and therefore it is parametrically justified and reliable.

TABLE II. Coefficients a and b in the δ expansion (50) for the reduction of the on-site magnetization for different values of the hopping parameters t' and t''.

Spiral state	t'	t''	a	b
(1,0)	−0.8	0.7	1.3	−1.9
(1,0)	−0.45	0.45	1.2	−1.3
(1,0)	−0.3	0.25	1.0	−0.7

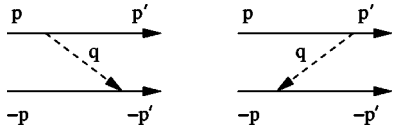

FIG. 9. Spin-wave exchange between holes leading to superconducting pairing.

VI. SUPERCONDUCTING PAIRING IN THE SPIRAL DUE TO SPIN-WAVE EXCHANGE

Now we investigate the possibility of superconducting pairing due to the spin-wave exchange shown in Fig. 9. We consider pairing between the states $\psi_{\mathbf{p}}$, Eq. (28), inside one full pocket (see the right-hand side in Fig. 3 for the (1,0) state). The corresponding many-body wave function has the form

$$|\Psi\rangle = \prod_{\mathbf{p}} (U_{\mathbf{p}} + V_{\mathbf{p}} \psi^\dagger_{\mathbf{p}} \psi^\dagger_{-\mathbf{p}})|0\rangle, \tag{51}$$

and represents pairing of spinless fermions. Within the full-pocket description the typical momentum transfer in the diagrams of Fig. 9 is $\mathbf{q}=\mathbf{p}-\mathbf{p}'$, $q=|\mathbf{q}| \sim p_F \propto \sqrt{\delta} \ll 1$. In the description with half pockets (left-hand side in Fig. 3) the momentum transfer is close to the antiferromagnetic vector $q \approx \mathbf{G}=(\pm\pi, \pm\pi)$. We use the full-pocket description which is more convenient, and in fact Eq. (51) already assumes such a description with $V_{-\mathbf{p}}=-V_{\mathbf{p}}$. Note that this condition does not mean that we consider negative parity pairing. Since parity is defined in the full magnetic Brillouin zone, in order to consider parity one needs to transfer back from the full-pocket description to the half-pocket description. Such a transition is related to translation by the antiferromagnetic vector $\mathbf{G}$. The wave function changes sign under such translation, $V_{\mathbf{k}}=-V_{\mathbf{k}+\mathbf{G}}$. Therefore $V_{-\mathbf{p}}=-V_{\mathbf{p}}$ implies that $V_{-\mathbf{k}}=+V_{-\mathbf{k}}$ and the pairing has positive parity. For a discussion of this peculiar symmetry property we refer the reader to Refs. 21 and 22.

Thus in the pairing channel the typical momentum transfer is $q \sim p_F \propto \sqrt{\delta}$. At such momentum transfer the spin-wave Green's function (42) is substantially different from the bare one (16). Its spectral weight $\mathrm{Im}D_\pi(\omega)$ is shifted from $\omega=\omega_{\mathbf{q}}=\sqrt{2}q \propto \sqrt{\delta}$ down to $\omega \sim \epsilon_F \propto \delta$. Unfortunately in this regime we cannot find an analytical solution for the pairing. Even at small δ one needs to solve the Eliashberg equations numerically and this is outside of the scope of the present work. However, we can put analytically a lower limit on the pairing and study its symmetry. To do so we replace the renormalized Green's function (42) in the diagrams of Fig. 9 by the bare Green's function (16). We call this approximation the "bare approximation" —it is similar to the one used in Ref. 22. The typical energy transfer in the diagrams of Fig. 9 is $\omega \sim \epsilon_F \propto \delta \ll \omega_{\mathbf{q}} \propto \sqrt{\delta}$. Therefore when calculating for the diagrams in Fig. 9, one can set $\omega=0$ in the spin-wave Green's function (16). This means that in the bare approximation it is sufficient to consider only the static interaction. By calculating for the diagrams in Fig. 9 with account of Eqs (16), (17), and (28) we find the effective pairing potential due to the spin-wave exchange:

$$V^{(dir)}_{\mathbf{p},\mathbf{p}'} = -\frac{M^2_{\mathbf{q}}}{\omega_{\mathbf{q}}} = -8Z^2t^2\frac{q_1^2}{q^2} = -8Z^2t^2\frac{(p_1-p_1')^2}{(\mathbf{p}-\mathbf{p}')^2}. \quad (52)$$

Recall that p_1 is the component orthogonal to the face of the magnetic Brillouin zone. Note that in agreement with the general Adler relation[25] $M_{\mathbf{q}} \to 0$, $q \to 0$ and hence the pairing potential remains finite at $q=0$, as was pointed out by Schrieffer.[26] In addition to the diagrams in Fig. 9 there are also exchange diagrams which differ by permutation of the legs. The total effective pairing potential due to the spin-wave exchange is then

$$V_{\mathbf{p},\mathbf{p}'} = V^{(dir)} - V^{(exch)} = 8Z^2t^2\left[-\frac{(p_1-p_1')^2}{(\mathbf{p}-\mathbf{p}')^2} + \frac{(p_1+p_1')^2}{(\mathbf{p}+\mathbf{p}')^2}\right]. \quad (53)$$

The BCS equation for the superconducting gap $\Delta_{\mathbf{p}} = -\Delta_{-\mathbf{p}}$ reads

$$\Delta_{\mathbf{p}} = -\frac{1}{4}\sum_{\mathbf{p}'} V_{\mathbf{p},\mathbf{p}'}\frac{\Delta_{\mathbf{p}'}}{E_{\mathbf{p}'}} = -\frac{1}{2}\sum_{\mathbf{p}'} V^{(dir)}_{\mathbf{p},\mathbf{p}'}\frac{\Delta_{\mathbf{p}'}}{E_{\mathbf{p}'}}, \quad (54)$$

where $E_{\mathbf{p}} = \sqrt{(\epsilon_{\mathbf{p}}-\mu)^2+\Delta^2_{\mathbf{p}}}$. Note that using the interaction (53) one has to put the coefficient 1/4 instead of 1/2 in the BCS equation to avoid double counting in the wave function (51). Alternatively one can use the standard form with 1/2 and with the direct interaction (52) only. In the weak-coupling limit the gap is small compared to the Fermi energy, therefore Eq. (54) can be solved in the vicinity of the Fermi surface ($\beta_1 p_1^2/2 + \beta_2 p_2^2/2 \approx \epsilon_F$) with logarithmic accuracy. The solution is discussed in Ref. 22 and we directly present the result:

$$\Delta_{\mathbf{p}} = \Delta_{SC} \sin m\phi,$$

$$\Delta_{SC} = C\epsilon_F e^{-1/g_m},$$

$$g_m = \frac{4Z^2t^2}{\pi\beta_2(\beta_1/\beta_2-1)}\left(\frac{\sqrt{\beta_1/\beta_2}-1}{\sqrt{\beta_1/\beta_2}+1}\right)^m. \quad (55)$$

Here Δ_{SC} is the maximum value of the superconducting gap. The angle ϕ is defined as

$$\sin\phi = \frac{\sqrt{\beta_2}p_2}{\sqrt{\beta_1 p_1^2 + \beta_2 p_2^2}}, \quad (56)$$

$m=1,2,3,\ldots$ is an integer number, and $C\sim 1$ is a constant. Equation (55) represents a family of solutions, however, the pairing is maximum in the channel with $m=1$. In this case, near the Fermi surface, the gap has the simple form (with p_1 and p_2 defined in Fig. 1),

$$\Delta_{\mathbf{p}} = \Delta_{SC}\frac{p_2}{\sqrt{(\beta_1/\beta_2)p_1^2+p_2^2}}. \quad (57)$$

We observe that there is a line of nodes along the (1,1) direction.

The solution (55) only describes the pairing within one full pocket while for a (1,0) spiral (which is of primary interest in the present work) there are two full pockets (Fig. 3).

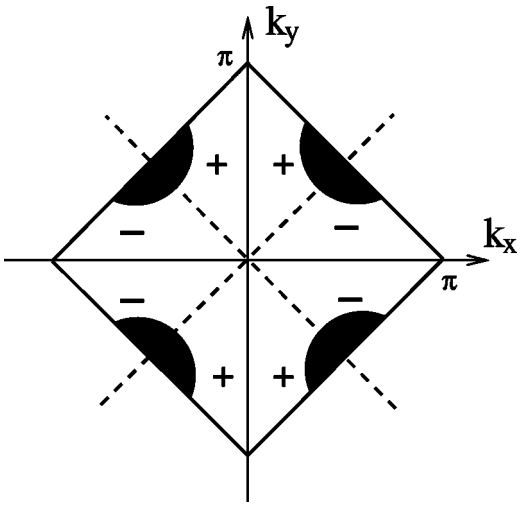

FIG. 10. *d* wave like symmetry of the superconducting gap in the (1,0) spiral state.

In this case one needs to solve the BCS equation numerically (i.e., take into account the pocket-pocket scattering) in order to determine the symmetry of the solution. This has been done for a similar problem in Ref. 23 and the expected result is shown in Fig. 10, where we also have gone back to the full Brillouin zone (half pocket) description. Since the symmetry of the lattice is spontaneously broken by the spiral, the "*d* wave" classification has lost meaning. In principle this should be reflected as an asymmetry of the pockets themselves; this asymmetry is small for $\delta \ll 1$ and is not shown in Fig. 10.

The pairing (55) obtained in the bare approximation is rather weak. As we have already mentioned the use of the exact spin-wave Green's function (42) is expected to enhance the pairing substantially due to the spectral weight shift towards low frequencies; we plan to discuss the full numerical solution of the Eliashberg equations in a future work. However, there exists an additional contribution to pairing [not accounted for in the solution (55)] which can be estimated already in the weak-coupling limit. This involves pairing via the upper φ band (ghost band) and can be included by replacing the many-body wave function (51) by

$$|\Psi\rangle = \prod_{\mathbf{p}}(U_{\mathbf{p}} + V_{\mathbf{p}}\psi^\dagger_{\mathbf{p}}\psi^\dagger_{-\mathbf{p}})\prod_{\mathbf{p}'}(\overline{U}_{\mathbf{p}'} + \overline{V}_{\mathbf{p}'}\varphi^\dagger_{\mathbf{p}'}\varphi^\dagger_{-\mathbf{p}'})|0\rangle. \quad (58)$$

To account for this effect we calculate the second-order correction to the spin-wave mediated interaction (52) between the ψ fermions. The correction is given by the diagram in Fig. 11. The dot in this diagram is given by Fig. 9 where the "flavor" of the fermion is changed from ψ to φ in each spin-wave vertex. Calculating for the diagrams in Fig. 9 with account of Eqs. (16), (17), and (28) we find that the dot is described by the same Eq. (52) but with a sign minus, "*dot*" $= M^2_{\mathbf{q}}/\omega_{\mathbf{q}} = 8Z^2t^2(p_1-l_1)^2/(\mathbf{p}-\mathbf{l})^2$. Hence the second-order correction Fig. 11 reads

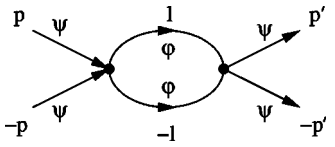

FIG. 11. Second-order correction to the pairing interaction between the ψ fermions due to virtual excitations to the empty φ band. The dot represents the spin-wave exchange shown in Fig. 9.

$$\delta V^{(dir)}_{\mathbf{p},\mathbf{p}'} = -(8Z^2t^2)^2 \sum_{\mathbf{l}} \frac{(p_1 - l_1)^2}{(\mathbf{p}-\mathbf{l})^2} \frac{1}{2\epsilon_{\mathbf{l}} + 2\Delta - 2\epsilon_F} \frac{(p'_1 - l_1)^2}{(\mathbf{p}'-\mathbf{l})^2}, \tag{59}$$

where $\epsilon_{\mathbf{l}}$ is given by Eq. (10), and ϵ_F and Δ are given by Eqs. (32) and (39) for the $(1,0)$ spiral state. The evaluation of the sum in Eq. (59) is particularly simple for the isotropic case, $\beta_1 = \beta_2$. We will consider this case for the purpose of an estimate of the effect. Using the expansion with Chebyshev polynomials $T_n(x)$

$$\frac{1}{1-2tx+t^2} = \frac{1}{1-t^2}[1 + 2\sum_{n=1}^{\infty} t^n T_n(x)], \tag{60}$$

and keeping only the first angular harmonic which is important for pairing in the $m=1$ channel, we obtain

$$\frac{(p_1 - l_1)^2}{(\mathbf{p}-\mathbf{l})^2} \to -\frac{1}{2}\frac{p_<}{p_>}\cos(\phi_p + \phi_l), \tag{61}$$

where $p_< = \min(p,l)$ and $p_> = \max(p,l)$. Using this representation and having in mind that in Eq. (59) $|p| = |p'| = p_F$ we perform the integration in Eq. (59) and find the correction to the pairing interaction:

$$\delta V^{(dir)}_{\mathbf{p},\mathbf{p}'} = -\frac{(8Z^2t^2)^2}{32\pi\beta}\left(1 - \frac{\Delta - \epsilon_F}{\epsilon_F}\ln\frac{\Delta}{\Delta - \epsilon_F} + \frac{\epsilon_F}{\Delta - \epsilon_F}\ln\frac{\Delta}{\epsilon_F}\right) \times (\cos\phi_p \cos\phi_{p'} + \sin\phi_p \sin\phi_{p'}). \tag{62}$$

We remind the reader that the above formula is valid in the isotropic case, $\beta = \beta_1 = \beta_2$. The correction (62) gives rise to an approximately 10% enhancement of the superconducting coupling constant g_1, Eq. (55):

$$\frac{\delta g_1}{g_1} = \frac{Z^2t^2}{2\pi\beta}\left(1 - \frac{\Delta - \epsilon_F}{\epsilon_F}\ln\frac{\Delta}{\Delta - \epsilon_F} + \frac{\epsilon_F}{\Delta - \epsilon_F}\ln\frac{\Delta}{\epsilon_F}\right). \tag{63}$$

This enhancement is an interesting qualitative effect related to the "ghost" band, but numerically its influence on pairing is relatively weak. Taking into account both Eqs. (55) and (63) we obtain the following estimate for the pairing in the dominant, $m=1$ channel [we use $\beta_1 = 2.9$, $\beta_2 = 3.8$ corresponding to the hoppings from Eq. (2), and also reinstate the Heisenberg exchange J]:

$$\Delta_{SC} \sim 10^{-2}\delta J. \tag{64}$$

For 10% percent doping this weak-coupling formula produces a $T_c \propto \Delta_{SC}$ of the order of several Kelvin which is about ten times smaller than transition temperatures in real compounds. The most important pairing enhancement is expected from the renormalization of the spin-wave Green's function, to be discussed in a separate work.

VII. CONCLUSIONS AND DISCUSSION

We have studied the phase diagram of the t-t'-t''-J model close to half filling. To determine the single hole properties (one hole injected in an antiferromagnetic background) we use the self-consistent Born approximation. This approximation is not parametrically justified for the t-J model, but it is known that it works remarkably well for the single-hole properties. The crucial observation is that these properties are not related to the long-range dynamics: all integrals in momentum space are convergent at large momenta (quantum fluctuations at distances 1–2 lattice spacings). Finite doping brings nontrivial long-range dynamics into the problem. To determine the dynamics we use the chiral perturbation theory which involves an expansion in powers of doping near half filling, $\delta \ll 1$. The efficiency of the chiral perturbation theory is in essence a consequence of the dimensionality of the problem (2+1 D) and Goldstone's theorem. We certainly cannot determine the exact value of doping so that it is small enough to justify the approach, but we claim that at sufficiently small δ the approach is parametrically justified. We show that the Neel state is unstable with respect to decay to spiral states as soon as doping is introduced. The analysis of the stability of the spiral phases is performed within the RPA approximation, and all nonRPA corrections are suppressed by powers of δ.

We find that at $t' = t'' = 0$ the spiral state is unstable toward a local enhancement of the spiral pitch, and consequently at that point the nature of the true ground state remains unclear. However, we have shown that for values of t' and t'' corresponding to real cuprates the (1,0) spiral state is stable. The phase diagram of the model at $t = 3.1$ (we set $J=1$) is shown in Fig. 5. For hole concentration $\delta \approx 0.119$ the (1,0) spiral is commensurate with the lattice with a period of eight lattice spacings, in agreement with experimental data. Figure 8 shows the dependence of the spiral on-site magnetization on doping. We demonstrate that spin-wave mediated superconductivity is developed above the spiral state and derive analytically a lower limit for the superconducting gap. One cannot classify the gap according to the lattice representations A_1, A_2, B_1, B_2, and E("s", "d", "p", $\cdots$) since the symmetry of the lattice is spontaneously broken by the spiral. However, the gap always has lines of nodes and a symmetry similar to d wave.

Finally we briefly discuss the possible connection of our results to experiments in the cuprates. Magnetic order has been observed in the superconducting states of both $La_{2-x-\delta}Nd_xSr_\delta CuO_4$ (Refs. 18 and 19) and $La_{2-\delta}Sr_\delta CuO_4$ (Ref. 14). This order seems to be particularly enhanced near the hole concentration $\delta = 1/8$ where a commensurate structure with a period of eight lattice spacings is observed. In addition, static charge order (with a period 4) has been observed at least in one of the materials.[18,19] This has lead to proposals that the state near $\delta = 1/8$ is a collinear spin density wave coexisting with a charge density wave (CDW) at twice the wave vector.[42] Such an interpretation of experiments

rules out a noncollinear spiral configuration of the type shown in Fig. 6, since the density of holes is expected to be uniform in the spiral case. On the other hand the question whether (static) charge order is a generic feature of the cuprates is far from being resolved and experiments in many cuprates are interpreted as showing fluctuating (i.e., dynamic) order in the charge sector.[45] For example, the existence of (static) charge order in $La_{2-\delta}Sr_{\delta}CuO_4$ is far less clear[14] although it also exhibits commensurate magnetic peaks around $\delta=1/8$.

In light of the above we find our result that the spiral (1,0) state is commensurate with the lattice (period 8, Fig. 6) for $\delta=0.119$ very promising. It seems to be consistent with the data in the magnetic sector (although the interpretation of Ref. 19 rules out a spiral state in that material). Moreover, it is known that doping introduces disorder, in turn leading to glassy features in the magnetism; at least at low doping (in the normal state) those features can be explained well within the spiral scenario.[15] In our opinion it would be also very interesting to study the density response of the system in the spiral state. In the context of the *t-J* model the density response has been recently investigated in the Neel state,[46] where fluctuations at energies of order J were found. In a spiral state, due to the presence of the ghost (empty) band, we expect that even lower energy charge-density fluctuations will exist, although a perfectly static CDW order seems impossible to stabilize. It is certainly more likely that some kind of order in the charge sector appears (if anywhere at all) around the point $t'=t''=0$, where the spiral state is inherently unstable. If we indeed interpret the region marked as "unstable" on our phase diagram in Fig. 5 as a candidate for such order, then the effect of increasing t' and/or t'' is to drive the system towards the (stable) spiral order, with a homogeneous charge distribution. This occurs for $|t'|/t \gtrsim 0.18$ (at $t''=0$). From this point of view our results are similar, at least superficially, to the DMRG results describing the destruction of stiped phases by second-neighbor hopping,[16,17] where a critical value of t' necessary to destabilize the stripes was found, and is quite close to our estimate above.

ACKNOWLEDGMENTS

We acknowledge discussions with J. Haase, G. Khaliullin, P. Horsch, C. Bernhard, and S. Sachdev. An important part of this work was done during the stay of one of us (O.P.S.) at the Max-Planck-Institut fur Festkorperforschung, Stuttgart. He is very grateful to all members of the theoretical department for hospitality and very stimulating atmosphere. O.P.S. also thanks the Institut de Physique Théorique (Université de Lausanne), where part of the research was performed, for hospitality and acknowledges support from the *Fondation Herbette*.

*E-mail: sushkov@phys.unsw.edu.au
†E-mail: Valeri.Kotov@ipt.unil.ch

[1] P. W. Anderson, Science **235**, 1196 (1987).
[2] V. J. Emery, Phys. Rev. Lett. **58**, 2794 (1987).
[3] F. C. Zhang and T. M. Rice, Phys. Rev. B **37**, 3759 (1988).
[4] B. I. Shraiman and E. D. Siggia, Phys. Rev. Lett. **62**, 1564 (1989).
[5] B. I. Shraiman and E. D. Siggia, Phys. Rev. B **46**, 8305 (1992).
[6] T. Dombre, J. Phys. (France) **51**, 847 (1990).
[7] C. L. Kane, P. A. Lee, T. K. Ng, B. Chakraborty, and N. Read, Phys. Rev. B **41**, 2653 (1990).
[8] A. Auerbach and B. E. Larson, Phys. Rev. B **43**, 7800 (1991).
[9] J. Igarashi and P. Fulde, Phys. Rev. B **45**, 10 419 (1992).
[10] H. Mori and M. Hamada, Phys. Rev. B **48**, 6242 (1993).
[11] A. V. Chubukov and K. A. Musaelian, Phys. Rev. B **51**, 12 605 (1995).
[12] B. Normand and P. A. Lee, Phys. Rev. B **51**, 15 519 (1995).
[13] L. O. Manuel and H. A. Ceccatto, Phys. Rev. B **61**, 3470 (2000).
[14] M.-H. Julien, Physica B **329-333**, 693 (2003).
[15] N. Hasselmann, A. H. Castro Neto, and C. Morais Smith, Phys. Rev. B **69**, 014424 (2004).
[16] S. R. White and D. J. Scalapino, Phys. Rev. B **60**, R753 (1999).
[17] T. Tohyama, C. Gazza, C. T. Shih, Y. C. Chen, T. K. Lee, S. Maekawa, and E. Dagotto, Phys. Rev. B **59**, R11 649 (1999).
[18] J. M. Tranquada, B. J. Sternlieb, J. D. Axe, Y. Nakamura, and S. Uchida, Nature (London) **375**, 561 (1995).
[19] J. M. Tranquada, J. D. Axe, N. Ichikawa, Y. Nakamura, S. Uchida, and B. Nachumi, Phys. Rev. B **54**, 7489 (1996).
[20] B. I. Shraiman and E. D. Siggia, Phys. Rev. B **40**, 9162 (1989).
[21] M. Yu. Kuchiev and O. P. Sushkov, Physica C **218**, 197 (1993).
[22] V. V. Flambaum, M. Yu. Kuchiev, and O. P. Sushkov, Physica C **227**, 267 (1994).
[23] V. I. Belinicher, A. L. Chernyshev, A. V. Dotsenko, and O. P. Sushkov, Phys. Rev. B **51**, 6076 (1995).
[24] See, e.g., S. Weinberg, Phys. Rev. Lett. **17**, 616 (1966); Phys. Rev. **166**, 1586 (1968). See also F. Hasenfratz and F. Niedermayer, Z. Phys. B: Condens. Matter **92**, 91 (1993), and references therein.
[25] S. L. Adler, Phys. Rev. **137**, B1022 (1965).
[26] J. R. Schrieffer, J. Low Temp. Phys. **99**, 397 (1995).
[27] Y. Tokura, S. Koshihara, T. Arima, H. Takagi, S. Ishibashi, T. Ido, and S. Uchida, Phys. Rev. B **41**, 11 657 (1990).
[28] M. Greven, R. J. Birgeneau, Y. Endoh, M. A. Kastner, B. Keimer, M. Matsuda, G. Shirane, and T. R. Thurston, Phys. Rev. Lett. **72**, 1096 (1994).
[29] O. K. Andersen, A. I. Liechtenstein, O. Jepsen, and F. Paulsen, J. Phys. Chem. Solids **56**, 1573 (1995).
[30] O. P. Sushkov, G. A. Sawatzky, R. Eder, and H. Eskes, Phys. Rev. B **56**, 11 769 (1997).
[31] S. Schmitt-Rink, C. M. Varma, and A. E. Ruckenstein, Phys. Rev. Lett. **60**, 2793 (1988).
[32] C. L. Kane, P. A. Lee, and N. Read, Phys. Rev. B **39**, 6880 (1989).
[33] G. Martinez and P. Horsch, Phys. Rev. B **44**, 317 (1991).
[34] Z. Liu and E. Manousakis, Phys. Rev. B **45**, 2425 (1992).
[35] E. Manousakis, Rev. Mod. Phys. **63**, 1 (1991).

[36] O. P. Sushkov and V. V. Flambaum, Physica C **206**, 269 (1993).
[37] D. Murray and O. P. Sushkov, Physica C **258**, 389 (1996).
[38] R. R. P. Singh, Phys. Rev. B **39**, 9760 (1989); Zheng Weihong, J. Oitmaa, and C. J. Hamer, *ibid.* **43**, 8321 (1991).
[39] R. Eder, Phys. Rev. B **43**, 10 706 (1991).
[40] H. Kimura, H. Matsushita, K. Hirota, Y. Endoh, K. Yamada, G. Shirane, Y. S. Lee, M. A. Kastner, and R. J. Birgeneau, Phys. Rev. B **61**, 14 366 (2000).
[41] S. Wakimoto, R. J. Birgeneau, Y. S. Lee, and G. Shirane, Phys. Rev. B **63**, 172501 (2001).
[42] S. Sachdev, Rev. Mod. Phys. **75**, 913 (2003), and references therein.
[43] S. Sachdev, Ann. Phys. (N.Y.) **303**, 226 (2003).
[44] Y. Hasegawa and D. Poilblanc, Phys. Rev. B **40**, 9035 (1989).
[45] S. A. Kivelson, I. P. Bindloss, E. Fradkin, V. Oganesyan, J. M. Tranquada, A. Kapitulnik, and C. Howald, Rev. Mod. Phys. **75**, 1201 (2003).
[46] P. Horsch, G. Khaliullin, and V. Oudovenko, Physica C **341-348**, 117 (2000).